ORIGINAL ARTICLE

Local mitigation of higher-order ionospheric effects in DFMC SBAS and system performance evaluation

Somkit Sophan[1] · Pornchai Supnithi[1] · Lin M. M. Myint[1] · Susumu Saito[2] · Kornyanat Hozumi[3] · Michi Nishioka[3]

Abstract

Dual-frequency multi-constellation (DFMC) satellite-based augmentation system (SBAS) is a new SBAS standard for aeronautical navigation systems. It supports aircraft navigation from the enroute to approach phases via the L1 and L5 frequencies (1575.42 and 1176.45 MHz). Although the ionosphere-free (IF) combination in the DFMC SBAS operation removes the first-order ionospheric delays in the pseudorange measurement, remaining terms including the satellite-clock offset errors and higher-order ionospheric (HOI) delays are still unaccounted for. The DFMC SBAS accuracy and integrity can be affected by the HOI effects, especially during severe ionospheric disturbances. In this work, we present the local DFMC SBAS corrections with and without the mitigation of HOI delays. We first estimate the HOI delay terms using the received pseudorange followed by separate satellite and receiver bias estimations based on the minimum sum-variance technique. The integrity terms can then be obtained. The performances of DFMC SBAS using the global navigation satellite system (GNSS) data including GPS, Galileo, and QZSS are evaluated using obtained GNSS data at stations in Thailand on the ionospheric quiet and disturbed days. The results show that with the HOI mitigation, the vertical positioning errors (VPE) on the quiet and disturbed days can be improved by 12% and 9%, whereas the vertical protection levels (VPL) are improved by 16% and 21%, respectively. In addition, we perform a preliminary assessment of DFMC SBAS based on the International Civil Aviation Organization (ICAO) requirements of two categories: Localizer Performance with Vertical guidance (LPV-200) and Category I precision approach (CAT-I) showing promising results.

Keywords DFMC SBAS · Higher-order ionospheric effects · GNSS · Single point positioning

✉ Pornchai Supnithi
pornchai.su@kmitl.ac.th

Somkit Sophan
61601026@kmitl.ac.th

Lin M. M. Myint
linminmin.my@kmitl.ac.th

Susumu Saito
susaito@mpat.go.jp

Kornyanat Hozumi
kukkai@nict.go.jp

Michi Nishioka
nishioka@nict.go.jp

1 School of Engineering, King Mongkut's Institute of Technology Ladkrabang, Bangkok 10520, Thailand

2 Navigation Systems Department, Electronic Navigation Research Institute, National Institute of Maritime, Port and Aviation Technology, Tokyo, Japan

3 National Institute of Information and Communications Technology Koganei, Tokyo 184-8795, Japan

Introduction

Satellite-based augmentation system (SBAS) is a well-known augmentation technique in aeronautical navigation in many parts of the world (European GNSS Agency 2018; Li et al. 2020). It is particularly a vital part of enroute and possibly approach phases. The SBAS components consist of the reference network, master station, uplink station, geostationary SBAS satellite and users. The master station generates the SBAS corrections and integrity by using the observed data from the reference network, and then sends them to the SBAS satellite via the uplink station. The benefits of the SBAS technology include the corrections of the user positioning errors, the guarantee of the user's availability, and the regional service. SBAS has been developed since 2003, when the global positioning system (GPS) satellites with L1 frequency are deployed such as the Wide Area Augmentation System (WAAS), ICAO SARPS (2006) and

RTCA DO-229D (2006). Recently, the developments of the global navigation satellite system (GNSS) have matured, the dual-frequency multi-constellation (DFMC) SBAS based on multi-constellation satellites receive more attention, for example, DFMC SBAS based on GPS (ICAO 2018; Reid et al. 2013a, b), BeiDou SBAS (BDSBAS) and Quasi-Zenith Satellite System (QZSS) used to augment GPS, GLONASS, and Galileo constellations (Zhao et al. 2020; Takahashi et al. 2022). The L1 SBAS system broadcasts the correction and integrity information via the L1 frequency (1575.42 MHz) including the fast and long-term (pseudorange and orbit) corrections and the ionospheric grid points (IGP). Recently, the new DFMC SBAS standard using both L1 and L5 (1176.45 MHz) frequencies has been proposed; the advantage lies on the fact that it cancels the ionospheric effects, broadcasts only the satellite clock-ephemeris corrections and integrity information, and avoids the high dilution-of-precision (DOP) effects.

In DFMC SBAS, the satellite clock-ephemeris corrections can be generated by the residual errors in the pseudorange measurements (Shao et al. 2020). Typically, the ionosphere-free (IF) carrier smoothing code technique with the raw data of the reference stations is utilized to estimate the residual errors of the pseudorange measurements between a satellite and a receiver. The locally dispersed reference stations with the triple difference (TD) technique, Sickle and Dutton (2020), are used to approximate the residual satellite-clock offset errors. Although the IF combination is used to remove the first-order ionospheric delays (Hoque and Jakowski 2007), the higher-order ionospheric (HOI) delays still remain in the pseudorange residual errors (Subirana et al. 2013). Exactly, the HOI delays can increase the residual errors up to 10 cm (Liu et al. 2016). Therefore, the positioning accuracy and integrity in DFMC SBAS can be degraded by the satellite clock-ephemeris corrections with the HOI delays as well as long baseline (Sophan et al. 2022).

The HOI delays in various systems have recently been investigated (Qi et al. 2021; Guo et al. 2023; Xi et al. 2021; Yehun et al. 2020). A typical approach is to estimate the HOI delays from the total electron content (TEC) parameters (Marques et al. 2011; Hadas et al. 2017) based on the geometry-free (GF) combination (Krypiak-Gregorczyk and Wielgosz 2018). The HOI delays with the Gravity Recovery and Climate Experiment Follow-On (GRACE-FO) observation are estimated based on the satellite-borne GPS technique to improve the precise orbit determination of GRACE-FO (Qi et al. 2021). The maximum precision improvement is observed at the millimeter levels. The HOI delays with the low-earth orbit (LEO) satellite observation are approximated by applying the International Reference Ionosphere-2016 (IRI-2016) and the International Geomagnetic Reference Field: the 13th generation (IGRF-13) models (Guo et al. 2023). Moreover, the HOI delays with the Beidou Navigation Satellite (BDS) are

analyzed by applying the TEC components of the IGRF-13 model and the Global Ionospheric Maps (GIM) model with the code pseudorange (Xi et al. 2021). The HOI effects can cause the user positioning errors in the ranges from 5 to 10 mm (Yehun et al. 2020).

To our knowledge, the local DFMC SBAS corrections with the HOI estimations or mitigations have not yet been considered in the previous research works. Therefore, in this work, we propose the procedures of local DFMC SBAS corrections together with the HOI delay mitigation. The HOI delays are computed from the local TEC values at stations in Thailand based on the Klobuchar model (Setti et al. 2019). In particular, the local DFMC SBAS corrections are generated by using the pseudorange residual errors of local reference stations with the minimum sum-variance and IF carrier smoothing code techniques. The system performances are evaluated on both quiet and disturbed days. Moreover, the availabilities of DFMC SBAS are evaluated for the Localizer Performance with Vertical guidance (LPV-200) and Category I precision approach (CAT-I) categories of the precise approach (PA) model (ICAO SARPS 2006).

In this article, the local DFMC SBAS corrections with the HOI delay mitigation have been derived in the background theory section. The methodology shows the simulation steps and data selections. In the simulation results, the DFMC SBAS corrections, user positioning errors, protection levels, and performances are illustrated in the results and discussions Section. Then, the conclusions are given at the end.

Background theories

User position estimations

The user coordinates and the receiver bias are typically calculated by using the single point positioning (SPP) algorithm based on the iterative weighted least-square estimation method (Takasu 2013). If the estimated user coordinate ($\hat{\mathbf{r}}_u = \left[\hat{x}_u, \hat{y}_u, \hat{z}_u\right]^T$) and the receiver bias ($\hat{b}_u$) are denoted as the column vector ($\hat{\mathbf{Z}} = \left[\hat{\mathbf{r}}_u, \hat{b}_u\right]^T$), the user position estimations of each time can be calculated by

$$\hat{\mathbf{Z}}_{k+1} = \hat{\mathbf{Z}}_k + \left(\mathbf{H}^T\mathbf{W}\mathbf{H}\right)^{-1}\mathbf{H}^T\mathbf{W}\left(\mathbf{Y} - h\left(\hat{\mathbf{Z}}_k\right)\right) \tag{1}$$

where k is the iterative index, and $h(\cdot)$ is the measurement vector function of errors, the coordinate unit matrix ($\mathbf{H}$) is

$$\mathbf{H} = \begin{bmatrix} -\frac{\boldsymbol{\rho}_u^1}{\|\boldsymbol{\rho}_u^1\|} & -\frac{\boldsymbol{\rho}_u^2}{\|\boldsymbol{\rho}_u^2\|} & \cdots & -\frac{\boldsymbol{\rho}_u^{N_s}}{\|\boldsymbol{\rho}_u^{N_s}\|} \\ 1 & 1 & \cdots & 1 \end{bmatrix}_{(4 \times N_s)} \tag{2}$$

where $\boldsymbol{\rho}_u^i$ is the column vectors of the equivalent geometric ranges between the satellite $i \in \left\{1, 2, \ldots, N_s\right\}$ and the user

based on the earth centered earth fixed (ECEF) coordinates system of the world geodetic system 1984 (WGS-84), i.e.,

$$\boldsymbol{\rho}_u^i = \left(\widehat{\mathbf{r}}_u^i + \boldsymbol{\delta}^i\right)^T - \widehat{\mathbf{r}}_u \tag{3}$$

$\widehat{\mathbf{r}}_u^i$ is the coordinate vectors ($\left[x_u^i, y_u^i, z_u^i\right]^T$) of the i th satellite estimated by the pseudorange at the user location, $\boldsymbol{\delta}^i$ is the satellite position error correction vectors ($\left[\delta x^i, \delta y^i, \delta z^i\right]^T$) of the DFMC SBAS corrections, and N_s is the total number of available satellites.

The weighting matrix ($\mathbf{W}$) is a square matrix. The diagonal matrix equals the inversion of the total errors for all available satellites as written by

$$\mathbf{W} = \text{diag}\left(\sigma_1^{-2}, \sigma_2^{-2}, \dots, \sigma_{N_s}^{-2}\right) \tag{4}$$

where σ_i^2, $i \in \left\{1, 2, \dots, N_s\right\}$, is the total variances of the available number of satellites N_s with the user at each time expressed as

$$\sigma_i^2 = \sigma_{i,DFRE}^2 + \sigma_{i,UIRE}^2 + \sigma_{i,tro}^2 + \sigma_{i,air\_DF}^2 \tag{5}$$

$\sigma_{i,DFRE}^2$ is the dual frequency range error (DFRE) variance of the i th satellite, $\sigma_{i,UIRE}^2$ is the ionospheric-free residual variance (user ionospheric range error: UIRE based on ICAO SARPs (2018) of the i th satellite with the user, $\sigma_{i,tro}^2$ is the variance of the tropospheric delay applied based on the minimum operational performance specification (MOPS), RTCA DO-229D (2006), σ_{i,air_DF}^2 is the variance of the airborne receiver errors for the dual frequency (L1-L5) modified from the single frequency of MOPS (Jie et al. 2018).

In addition, the observed vectors ($\mathbf{Y}$) of all available satellites with the user equal

$$\mathbf{Y} = \begin{bmatrix} R_u^1 + c\widehat{\Delta t}_u^1 - \widehat{\delta T}_u^1 - \widehat{\delta \Delta I}_u^1 \\ R_u^2 + c\widehat{\Delta t}_u^2 - \widehat{\delta T}_u^2 - \widehat{\delta \Delta I}_u^2 \\ \vdots \\ R_u^{N_s} + c\widehat{\Delta t}_u^{N_s} - \widehat{\delta T}_u^{N_s} - \widehat{\delta \Delta I}_u^{N_s} \end{bmatrix}_{(N_s \times 1)} \tag{6}$$

where R_u^i is the smoothed pseudorange measurements (in meter) between the u-th user and the i-th satellites, where $i \in \left\{1, 2, \dots, N_s\right\}$ based on ICAO SARPs (ICAO 2018), c is the speed of light in the vacuum (in meters/sec), $\widehat{\Delta t}_u^i$ is the i th satellite-clock offset (in sec) estimated by the code pseudorange at the user, $\widehat{\delta T}_u^i$ is the tropospheric delay (in meter) of the i th satellite estimated based on MOPS, RTCA DO-229D (2006), with the user, and $\widehat{\delta \Delta I}_u^i$ is the HOI delays (in meter) for the i th satellite with the user estimated from the local TECs based on the Klobuchar model (Setti et al. 2019). The HOI delays are derived by Marques et al. (2011), Hadas et al. (2017), and Qi et al. (2021). Additionally, the local DFMC SBAS corrections without and with the HOI

mitigations are investigated. In the case without HOI mitigations, the $\widehat{\delta \Delta I}_u^i$ term for the available satellites in (6) will be omitted.

Local DFMC SBAS corrections

The DFMC SBAS corrections based on ICAO (2018) consist of the error corrections of satellite-position and satellite-clock errors. Typically, the satellite-position error correction is utilized to correct the satellite coordinate vectors in (3) whereas the satellite-clock error correction is used to reduce the estimated satellite-clock offset errors in (6). These corrections are broadcast via the geostationary SBAS satellite. The information is composed of several message types (MT) explained in ICAO (2018). The MT31-32 and MT34-37 are designed to support the DFMC SBAS service. In this work, we evaluate the performance without the SBAS satellites, the DFMC SBAS corrections have not been encoded into the message format.

The proposed local DFMC SBAS corrections with the HOI mitigations are described in the four steps as follows.

Step 1: Given the precise coordinate vectors of the receiver, the residual errors between the i th satellite and the j th receiver (ΔR_j^i) can be expressed below.

Method A (baseline): The residual errors ($\Delta R_{j,A}^i$) at each time *including* the HOI effects are computed from

$$\begin{aligned} \Delta R_{j,A}^i &= R_j^i - \left\| \mathbf{r}_j^i - \mathbf{r}_j \right\| + c\widehat{\Delta t}_j^i - \widehat{\delta T}_j^i \\ &= \underbrace{c\Delta t_j}_{\beta_j} + \underbrace{\left(\delta \Delta I_j^i - c\delta \Delta t_j^i + \varepsilon_j^i\right)}_{\beta_{j,A}^i} \end{aligned} \tag{7}$$

where R_j^i is the smoothed pseudorange measurements between the i th satellite and the j th receiver based on ICAO SARPs (ICAO 2018), $\mathbf{r}_j^i$ is the coordinate vectors (in meter) of the i th satellite estimated by the code pseudorange at the j th receiver ($\left[x_j^i, y_j^i, z_j^i\right]$), and $\mathbf{r}_j$ is the precise coordinate vectors of the j th receiver ($\left[x_j, y_j, z_j\right]$), $\widehat{\Delta t}_j^i$ is the i th satellite clock offset (in sec) estimated by the code pseudorange at the j th receiver, $\widehat{\delta T}_j^i$ is the tropospheric delay of the i th satellite estimated based on MOPS (RTCA DO-229D, 2006) with the j th receiver, β_j is the j th receiver biases (in meters), $\delta \Delta t_j^i$ is the residual satellite-clock offset errors of the i th satellite at the j th receiver (in sec), $\delta \Delta I_j^i$ is the HOI delays (in meter) for the i th satellite with the j th receiver, ε_j^i is the total errors (in meter) of the estimated parameters, difference code biases, and smoothed errors, and $\beta_{j,A}^i$ is the residual errors of the $\delta \Delta I_j^i$, $\delta \Delta t_j^i$, and ε_j^i parameters for the i th satellite with the j th receiver. Note that t he $c\delta \Delta t^i$ term

for the i th satellite is equivalent to the satellite-clock error correction of DFMC SBAS.

Method B (proposed): The residual errors ($\Delta R^i_{j,B}$) of each time *excluding* the HOI effects are calculated by

$$\Delta R^i_{j,B} = \Delta R^i_{j,A} - \widehat{\delta \Delta I}^i_j = \underbrace{c\Delta t_j}_{\beta_j} - \underbrace{\left(c\delta \Delta t^i_j - \varepsilon^i_j\right)}_{\beta^i_{j,B}} \tag{8}$$

where $\widehat{\delta \Delta I}^i_j$ is the estimated HOI delays for the i th satellite with the j th receiver estimated from the local TECs based on the Klobuchar model (Setti et al. 2019), and $\beta^i_{j,B}$ is the i th satellite biases with the j th receiver excluding the HOI effects (in meters).

Step 2: From step 1, the β_j term should be approximated before the $\beta^i_{j,A}$ term since the precise receiver coordinates can be calculated by historical data. Empirically, the β_j should be the constant value for a short period (i.e., 5 min) due to the fixed receiver. In this work, the minimum sum-variance technique is applied to the TD observations (between-satellites, between-receivers, and between-epochs). Then each receiver j th ($\widehat{\beta}_j$) at time t can be approximated by

$$\widehat{\beta}_j(t) \approx \min_{X_{min} \leq b_j \leq X_{max}} \left(\sum_{i=1}^{N_s} \sum_{\tau=1}^{N_\tau} \frac{\left(\Delta R^i_{j,A}(t-\tau) - b_j\right)^2}{N_s + N_\tau} \right) \tag{9}$$

where X_{min} and X_{max} are the minimum and maximum values of the $\Delta R^i_{j,A}$ at the time in $\{t-1, t-2, \ldots, t-N_\tau\}$, b_j is an arbitrary mean value selected from min-to-max values, and N_τ is the time window size. The β_j value is approximated depending on the N_τ and N_s parameters. The N_s parameter requires at least three satellites since the optimal mean can be computed. Additionally, the satellite and receiver coordinates are based on the WGS-84 ECEF coordinate system, Takasu (2013).

Step 3: Once the β_j in (9) is obtained, the remaining term of $\beta^i_{j,A}$ corresponding the i th satellite with the reference receiver j th are computed. Since the baselines between the reference receivers for the SBAS ground segment are generally more than 100 km, the $\beta^i_{j,A}$ are estimated by the different values. Hence, in this work, the minimum sum-variance technique is also applied to the TD observations. The mean values of each satellite i th ($\widehat{\beta}^i$) at time t are estimated from

$$\widehat{\beta}^i(t) \approx \min_{Q_{min} \leq b^i \leq Q_{max}} \left(\sum_{j=1}^{N_r} \sum_{\tau=1}^{N_\tau} \frac{\left(\widehat{\beta}^i_{j,A}(t-\tau) - b^i\right)^2}{N_r + N_\tau} \right) \tag{10}$$

where $\widehat{\beta}^i_{j,A}$ is the remaining term of $\Delta R^i_{j,A} - \widehat{\beta}_j$ at time t, Q_{min} and Q_{max} are the minimum and maximum values of the $\widehat{\beta}^i_j(t)$

where $j \in \{1, 2, \ldots, N_r\}$, N_r is the total number of available receivers, and b^i is the arbitrary mean value selected from the min-to-max values. Additionally, the method B is also computed similar to the method A by changing the $\Delta R^i_{j,A}$ to $\Delta R^i_{j,B}$ and $\beta^i_{j,A}$ to $\beta^i_{j,B}$ instead.

Equations (9) is utilized to observe the $\widehat{\beta}^i_j$ of the i th satellites (multi-constellation) at the receivers j th, and (10) is applied to optimize the $\widehat{\beta}^i$ values by using the $\widehat{\beta}^i_j$ of many reference receivers with the long baselines. Thus, the ε^i_j parameter should be reduced by the minimum sum-variance technique with the TD observations.

Step 4: The $\widehat{\beta}^i$ values, equivalent to the residual satellite-clock offset errors of i th satellite, cause the errors of the satellite coordinate vector interpolations (based on by the code pseudorange at each receiver). Hence, the local DFMC SBAS corrections, the i th satellite position error correction vectors ($\boldsymbol{\delta}^i$) can be generated from the $\widehat{\beta}^i$ values. They are projected to the (X,Y,Z) coordinate by using the unit vectors of the virtual satellite coordinates. The $\boldsymbol{\delta}^i$ vectors of the i th satellite at each time can be computed from

$$\boldsymbol{\delta}^i = \frac{\mathbf{r}^i}{\|\mathbf{r}^i\|} \times \widehat{\beta}^i \tag{11}$$

where $\mathbf{r}^i$ is the virtual coordinate vectors of the i th satellite ($[x^i, y^i, z^i]$) approximated by the code pseudorange at the master station.

DFMC SBAS integrity

The integrity parameters are utilized to determine the availabilities of the SBAS operation (RTCA DO-229D 2006). In practice, the horizontal protection level (HPL) and the vertical protection level (VPL) for the PA model at each time are, respectively, computed by

$$HPL = K_H \times \sqrt{\frac{d_E^2 + d_N^2}{2} + \sqrt{\left(\frac{d_E^2 - d_N^2}{2}\right)^2 + d_{EN}^2}} \tag{12}$$

and

$$VPL = K_V \times d_U \tag{13}$$

where K_H and K_V are the constant values of HPL and VPL, d_E^2 and d_N^2 are the variances of the true error distribution in the east and north axis, respectively, d_{EN}^2 is the covariance of the true error distribution in the east-north axis, d_U is the standard deviation of the true error distribution in the up-axis. The true error distribution can be calculated by utilizing the inversion of the geometry matrix and weighting matrix derived in RTCA DO-229D (2006).

From (4)-(5), the weighting matrix $\mathbf{W}$ is computed from the total variances including the DFRE values (in meters). They can be calculated based on the projection method with the observed data of the reference stations derived by Shao et al. (2020). This technique can bound the satellite correction errors as 99.9% of the time; it is also suitable for use in the multi-constellation. Hence, the DFRE values can be computed from

$$\sigma_{i,DFRE} = \sqrt{\left(\sqrt{\lambda_1} + \sqrt{\mathcal{C}_i}\right)^2 - \mathcal{C}_i^2 + C_{i,t}} \qquad (14)$$

where λ_1 is the maximal distance from the point on the ellipsoidal surface to the origin, $\mathcal{C}_i$ equals $\mathbf{C}_{i,ot}^T \mathbf{C}_{i,o}^{-1} \mathbf{C}_{i,ot}$, and $C_{i,t}$ is the inversion of the i th satellite clock variance. The covariance matrix ($\mathbf{C}_{i,o,(3\times3)}$, $\mathbf{C}_{i,ot,(3\times1)}$, and $C_{i,t}$) of the i th satellite orbit coordinate (o) with the clock error (t) is

$$\begin{bmatrix} \mathbf{C}_{i,o} & \mathbf{C}_{i,ot} \\ \mathbf{C}_{i,ot}^T & C_{i,t} \end{bmatrix}_{(4\times4)} = \left(\mathbf{A}_i^T \mathbf{\Lambda}_i \mathbf{A}_i\right)^{-1} \qquad (15)$$

$\mathbf{A}_i$ is the unit vector matrix ($4 \times N_r$) of the i th satellite position error correction vectors with the j th receiver ($\left[\delta x_j^i, \delta y_j^i, \delta z_j^i, 1\right]^T$), and $\mathbf{\Lambda}_i$ is the weighting matrix where the diagonal matrix is the inversion of variances in the i th satellite-clock offset errors depending on the N_r and N_τ parameters.

Methodology

In this work, the local DFMC SBAS corrections are generated based on the method A and B. We evaluate the system with and without the HOI delays on both ionospheric quiet and disturbed days.

System simulations

The assessments of DFMC SBAS are demonstrated in Fig. 1 consisting of six steps. First, the raw observations are fed as input. The first-order ionospheric delays are removed by the IF combinations. Second, the multipath noise is typically removed by the elevation mask component, whereby the satellites below the elevation mask are cut-off. Third, the IF carrier smoothing code technique is utilized to approximate the pseudorange measurements. Fourth, this step, both method A and B are tested. For method A, the satellite position error correction vectors and the integrity parameters are generated (Eq. 11,14) based on the residual errors including the HOI effects (Eq. 7), however, for method B, they are based on the residual errors with the HOI effects removed (Eq. 8). Fifth, the user coordinate vectors are calculated
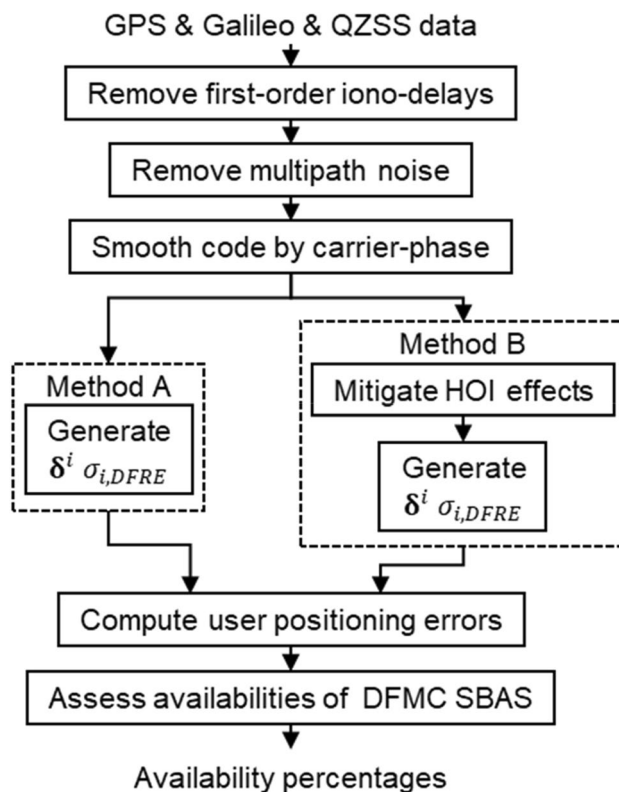

Fig. 1 Block diagram of the DFMC SBAS assessments (Method A represents a baseline method, whereas Method B is the proposed method with additional HOI mitigation)

Table 1 Important parameters for the DFMC SBAS simulation

Items	Values
Observed periods:	Date of year (DOY) in 2022:
Quiet days	36, 38, 45, and 50 (5th, 7th, 14th, and 19th in February)
Disturbed days	60, 62, 74, and 75 (1st, 3rd, 15th, and 16th in March)
Sampling time	1 s
Updating time	6 s
Elevation mask	15°
N_τ	300 samples (5 min)

based on the SPP algorithm in (1), then the horizontal positioning errors (HPE) and vertical positioning errors (VPE) are computed based on the Haversine formula. Finally, the available percentages of DFMC SBAS are assessed by comparing the HPE and VPE values with the HPL and VPL values, respectively, on the Stanford diagram (Ogier 2021).

In the simulations, the important parameters are described in Table 1. To investigate the HOI mitigation on DFMC SBAS, the quiet and disturbed days are selected based on the rate of TEC index (ROTI) values without the

geomagnetic storms (the Dst above -30, Nose et al. 2015, and the Kp below 3, Jürgen et al. 2021). Then the observed periods of four days (non-consecutive) are considered explaining in Subsection-dataset. Normally, an observed sample is defined as 1 s, the SBAS service updated at least every 6 s (updating time) can be done. The elevation mask is defined as 15°, which is suitable for the multi-constellation case. Additionally, the N_τ of 300 samples (5 min) is a suitable sample for estimating the $\hat{\beta}_j$ values in the near real-time processing.

Figure 2 shows the selected stations covering Thailand. The reference stations include CHAN, CHMA, DPT9, NKSW, PJRK, SISK, SOKA, and UDON. The remaining three stations (CNBR, UTTD, and SRTN) are considered as the users. Since the DPT9 station is selected as the master station, distances between the master and user (CNBR, UTTD, and SRTN) stations are about 60, 432, and 529 km, respectively.
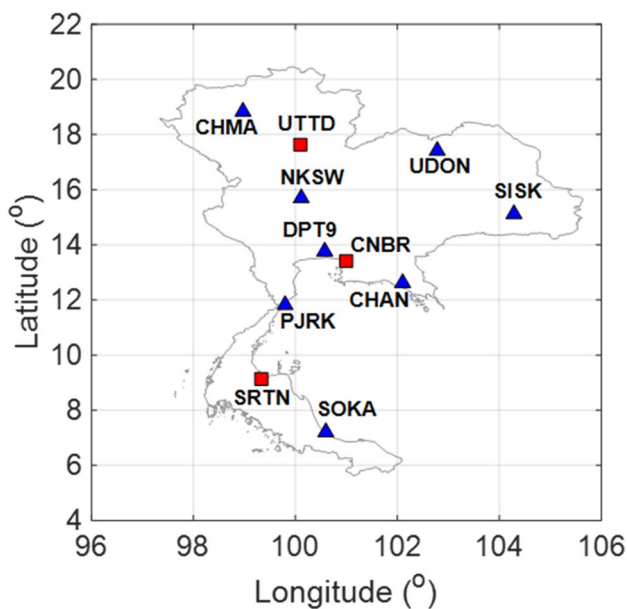
Dataset

In the simulations, the GPS, Galileo, and QZSS satellites are utilized in the band of L1 and L5 frequencies. The GPS and Galileo satellites are in a medium earth orbit (MEO), however, the QZSS satellite is in a quasi-zenith orbit (QZO). Currently, the BDS-3 satellites with same bands are available, however, the BeiDou data are not available from the selected reference stations. Since not all GPS satellites broadcast the L5 frequency at present, fewer than four satellites are available at times. For example, at 12:00 and 22:30 h (local time: LT), three core systems with both L1 and L5 are illustrated in Fig. 3. The distinct colors indicate each constellation, i.e., GPS (G, O), Galileo (E, □), and QZSS (J, ◇) satellites. Normally, the GPS satellites during 12:00 LT have six satellites, but during 22:30 LT, only one satellite is available. Hence, the Galileo and QZSS satellites are utilized to avoid the positioning outage as well as the high DOP effects.

Figure 4 shows the ROTI values of the CNBR station. The top figure (quiet days) consists of the DOY of the 36, 38, 45, and 50 in 2022 labeled as the day numbers of the 1 to 4, respectively. Each ROTI line is computed by the time window of 5 min and the elevation masks of 30°. The data gap is due to missing observational data. Similarly, the bottom figure (disturbed days) shows the DOY of the 60, 62, 74, and 75 in 2022. Normally, the ROTIs on the quiet days are below 0.5 TECU/min with low fluctuation, whereas on the disturbed days are above 0.5 TECU/min after sunset (Schaer

Fig. 2 Locations of the reference (△) and user (□) stations in Thailand (https://gnss-portal.rtsd.mi.th/)

Fig. 3 Sky plots of the GPS (G, O), Galileo (E, □), and QZSS (J, ◇) satellites with both L1 and L5 at 12:00 LT (left) and 22:30 LT (right)
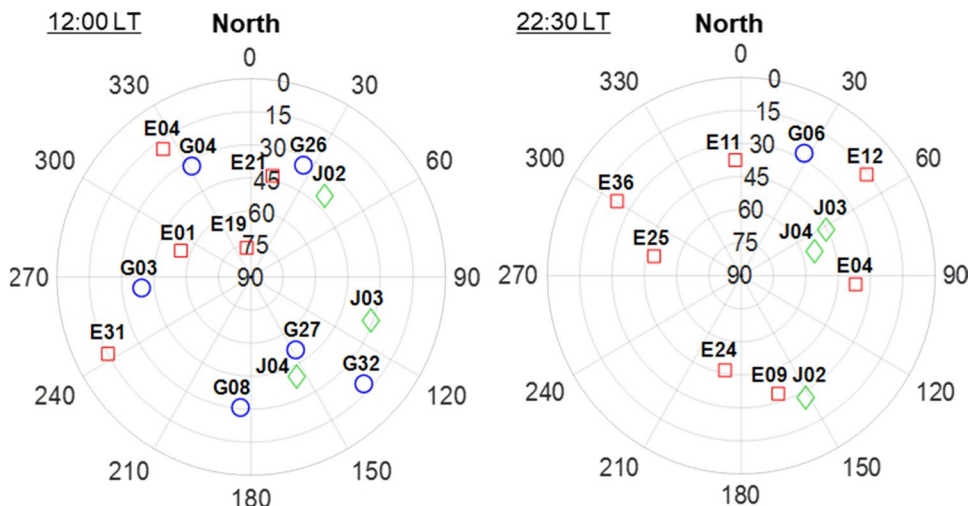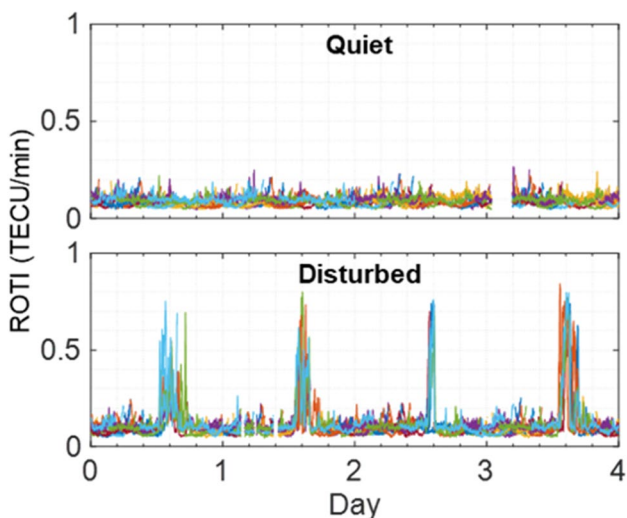
Fig. 4 ROTI plots of the CNBR station on the quiet (top) and disturbed (bottom) days (Day 1 to 4 represents DOY 36, 38, 45, and 50 in 2022)
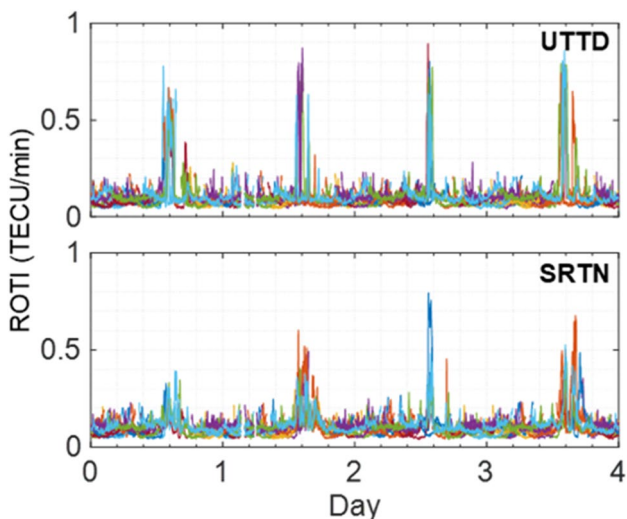
Fig. 5 ROTI plots of the UTTD (top) and SRTN (bottom) stations on the disturbed days (Day 1 to 4 represents DOY 36, 38, 45, and 50 in 2022)

1999). Although there is no geomagnetic storm on the disturbed days during the studied period, the ROTIs after sunset indicate local ionospheric disturbances due to the equatorial plasma bubbles (EPB).

Similarly, Fig. 5 shows the ROTI plots at UTTD and SRTN stations. Mostly, the ROTIs with the large fluctuation are observed after sunset. At the SRTN station, relatively lower ROTI levels are seen on the first day. Interestingly, the SRTN station generally experiences lower ROTIs than the UTTD station. These results indicate that the ionospheric disturbances vary by location.

Results and discussions

The DFMC SBAS availabilities with the quiet and disturbed events are evaluated. The local DFMC SBAS correction and integrity with and without the HOI delays are utilized for the user segments such as the CNBR, SRTN, and UTTD stations in Fig. 2. Then the simulation results are demonstrated and discussed as follows.

DFMC SBAS parameters

Figure 6 shows the satellite position error correction $(\delta x^i, \delta y^i, \delta z^i)$ and integrity parameter $(\sigma_{i,DFRE})$ from the method B on the quiet days. The six reference stations (CHAN, CHMA, DPT9, NKSW, PJRK, and UDON) are utilized for the computation of the master station processing. The distinct color lines indicate each satellite number of the GPS (G04 and G10), Galileo (E02 and E03), and QZSS (J02 and J03) constellation. The satellite position error correction vectors $(\boldsymbol{\delta}^i)$ are computed by (11) with the virtual coordinate vectors of the i th satellite approximated by the
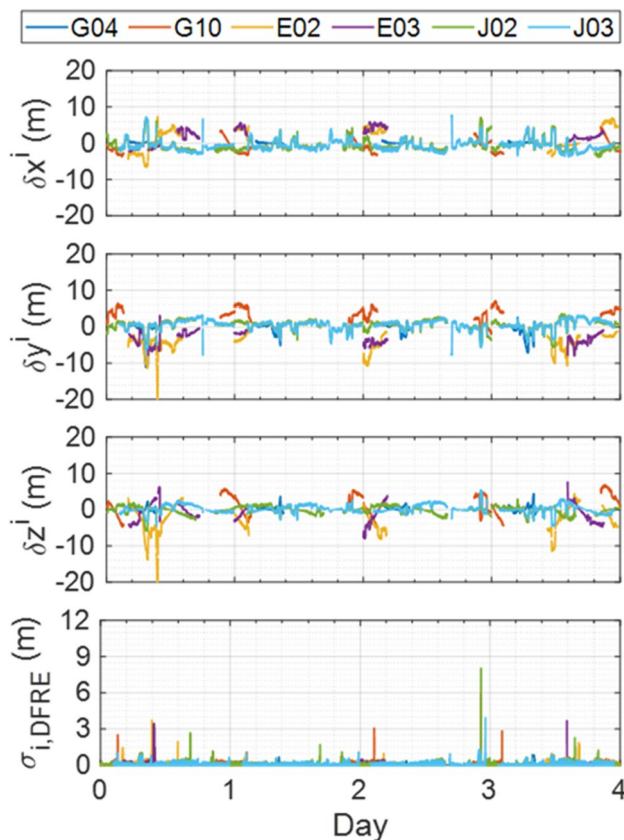
Fig. 6 Satellite position error correction and integrity parameter with the method B for each satellite on the quiet days (Day 1 to 4 represents DOY 36, 38, 45, and 50 in 2022)

code pseudorange at DPT9, while the integrity parameters ($\sigma_{i,DFRE}$) are calculated by (14).

In Fig. 6, the δx^i, δy^i, and δz^i values are within ± 10 m. The position error correction of J02 and J03 show the least fluctuations (± 2 m), possibly due to the trajectory of the quasi-zenith orbit (QZO) with the local quiet event. The $\sigma_{i,DFRE}$ values are more than 3 m are caused from some spikes or outliers of the position error correction. For example, δy^i and δz^i vectors of E02 and E03 are on the first day. Hence, the $\sigma_{i,DFRE}$ parameter is utilized as the error indicator related to the local DFMC SBAS corrections.

Figure 7 shows the 95th percentile of $\sigma_{i,DFRE}$ versus the number of reference stations (4, 6 and 8) for each satellite. The distinct color bars are computed on four days, whereby the dotted bars are the averages of all color bars. On the quiet days, the $\sigma_{i,DFRE}$ values of each satellite are obviously decreased as the number of reference stations increases showing the averaged $\sigma_{i,DFRE}$ of 1.08, 0.26, and 0.12 m for 4, 6, and 8 reference stations, respectively. On the disturbed days, the similar trend of $\sigma_{i,DFRE}$ are still seen, however, the averaged $\sigma_{i,DFRE}$ are relatively larger compared with the quiet days. In the following analysis, we select the number of the reference stations to be 6.

User positioning errors

The preliminary DFMC SBAS operation can be evaluated by the user positioning errors (user processing). The precise coordinate vectors of the reference station are defined by the AUSPOS Online GPS Processing Service on the website https://gnss.ga.gov.au/auspos. This website is administered by Geoscience Australia; the users need to submit the observed data with the receiver independent exchange format (RINEX). The raw GPS pseudorange values are utilized with the reference stations of the international GNSS service (IGS) and the Asia Pacific Reference Frame (APREF) to compute the precise receiver coordinate based on the double-difference strategy (relative positioning); the accuracy is in the centimeter levels. Then an AUSPOS report will be emailed to users with the Geocentric Datum of Australia 2020 (GDA2020), Geocentric Datum of Australia 1994 (GDA94), and International Terrestrial Reference Frame (ITRF) coordinates. Further information is described by Malys and Slater (1994). Figure 8 shows the number of satellites, HPE, and VPE at the user station (CNBR) processing on the quiet and disturbed days. The 'SPS' legend indicates the standard positioning system (SPS) based on the GPS L1 frequency and the Klobuchar model, whereas the 'DFMC SBAS-A' and 'DFMC SBAS-B' legends represent the method A and B, respectively. The SPS method is used to validate the DFMC SBAS algorithm. On the quiet days, the number of available satellites with both L1 and L5 tends to decrease from after sunset to midnight. The HPEs are

typically lower than 5 m, but the VPEs are typically 10 m or less. As expected, the VPEs are higher than HPEs by about 1.5 m due to the geography and ionospheric delays. Both HPE and VPE increase significantly as the number of satellites decreases. Importantly, the DFMC SBAS-B method can better improve the errors than the DFMC SBAS-A.

For ease of comparison, the 95th percentile of HPE and VPE at three stations (CNBR, UTTD, SRTN) are summarized in Fig. 9. Each graph is obtained from the positioning errors for four days. On the quiet days, both the HPEs and VPEs from the method B are relatively lower than the method A. Compared with DFMC SBAS-A, the DFMC SBAS-B method can improve the HPEs at the CNBR, UTTD, and SRTN stations by 0.14 (13%), 0.07 (11%), and 0.05 (5%) m, and the VPEs about 0.21 (8%), 0.15 (12%), and 0.16 (10%) m, respectively. The improved percentage is computed by $(1 - (\text{DFMC SBAS-B}/\text{DFMC SBAS-A})) \times 100\%$. Similarly, on the disturbed days, the HPEs and VPEs of each user station are also improved, but the improvements are slightly less. The HPEs of the DFMC SBAS-B over DFMC SBAS-A results are about 0.12 (10%), 0.07 (10%), and 0.05 (5%) m at the CNBR, UTTD, and SRTN stations, respectively. While the VPEs at the CNBR, UTTD, and SRTN stations are about 0.25 (8%), 0.13 (8%), and 0.15 (7%) m, respectively. The improvement due to Method B illustrates that when the HOI effects are mitigated, the positioning errors are reduced by 5–20 cm.

Here, we provide some discussions on the results in Fig. 9, the DFMC SBAS corrections with the local HOI mitigation can significantly enhance the user positioning accuracy on both quiet and disturbed days in the range of 7%-13%, but the improvements on the disturbed days
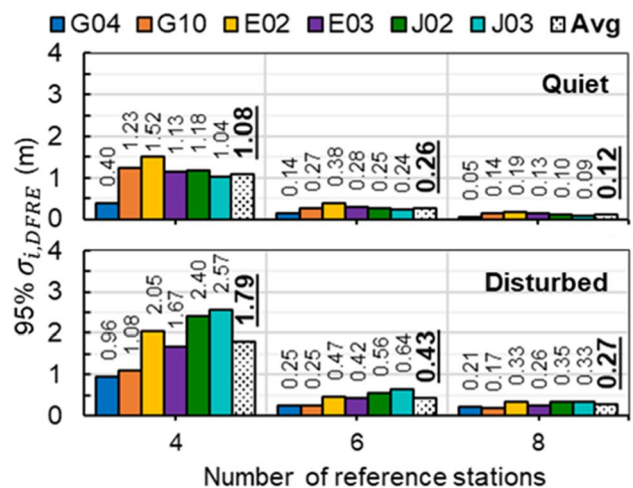

Fig. 7 The 95th percentile of $\sigma_{i,DFRE}$ and averages (Avg) based on the method B versus the number of reference stations on the quiet (top) and disturbed (bottom) days

Fig. 8 Number of satellites (top panel) and user positioning errors of the SPS, DFMC SBAS-A, and DFMC SBAS-B methods in terms of HPE (middle panel) and VPE (bottom panel) on the quiet (left panel) and disturbed (right panel) days at CNBR station (Day 1 to 4 represents DOY 36, 38, 45, and 50 in 2022)
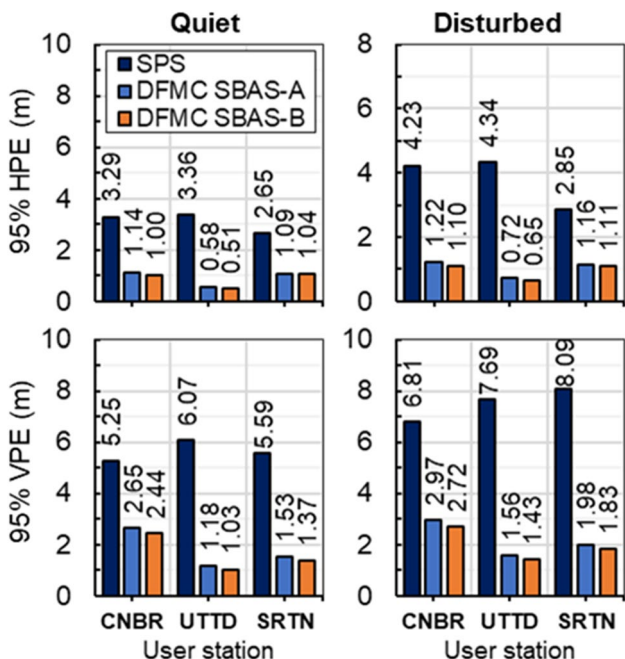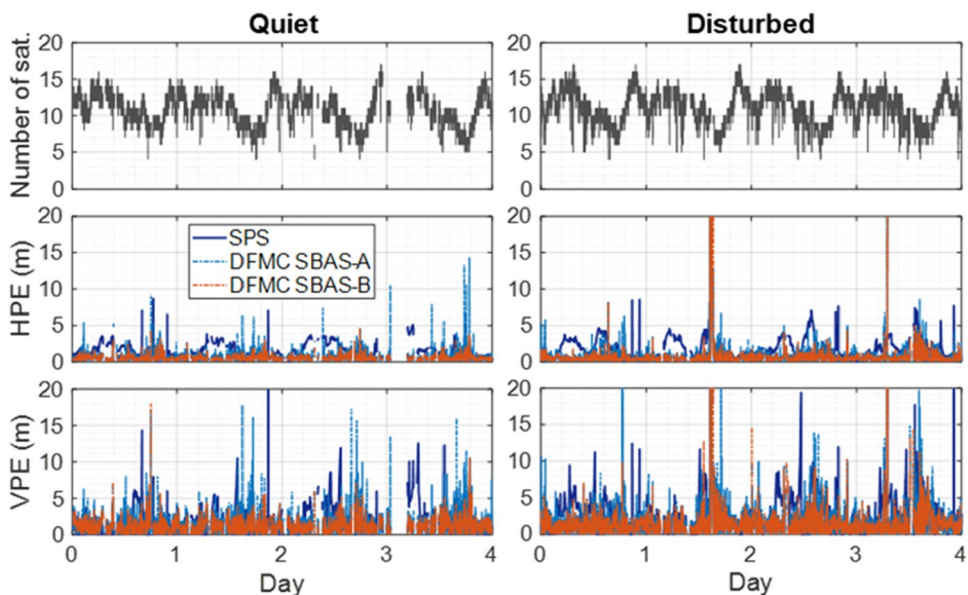
Fig. 9 User positioning errors in the 95.th percentile HPE (top panel) and VPE (bottom panel) on the quiet (left panel) and disturbed (right panel) days for three user stations (CNBR, UTTD, and SRTN)

are slightly smaller than those on the quiet days by about 2%. It is clear from the results in Fig. 7 (disturbed), larger HOI delays are observed for any number of reference stations. Therefore, the estimated HOI delays on the disturbed days are less reliable than on the quiet days leading to the degradation on the precision of the DFMC SBAS corrections. Since we estimate the HOI values from Klobuchar model, more accurate HOI can be obtained from the actual pseudorange observations.
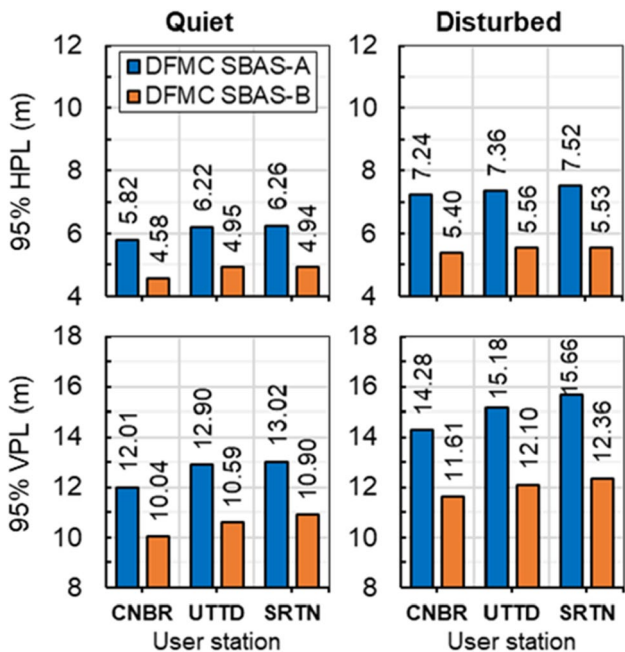
Protection levels

In practice, the HPL and VPL, rather than HPE and VPE values are estimated by the airborne receivers since actual positions are not known. These values can be utilized to assess the availability of the SBAS operation. Figure 10 shows the number of satellites, HPL, and VPL results of the user station (CNBR) computed by (12) and (13) with $K_H = 6.0$ and $K_V = 5.33$, respectively. Similar trends in HPL and VPL are also seen here, showing the increased protection levels up to 40 and almost 60 m, respectively, when the number of satellites is decreased below 10. Similar to Fig. 9, the protection levels (PL) based on the 95th percentile are summarized in Fig. 11.

In Fig. 11, we investigate the HPLs and VPLs similarly to Fig. 10 for the three stations. On the quiet days, the HPLs and VPLs with the HOI effects for all user stations can be reduced by the DFMC SBAS-B method by about 21% and 16%, respectively. In contrast, on the disturbed days, the improved HPLs with DFMC SBAS-B for the CNBR, UTTD, and SRTN stations are about 25%, 24%, and 26%, while the improved VPLs are about 19%, 20%, and 21%, respectively. Similarly, the protection levels follow the trends of the user positioning errors in Fig. 9, but the improvements on the disturbed days are slightly larger than those on the quiet days. It is reasonable that the large HOI delays on the disturbed days caused the overestimated protection levels with DFMC SBAS-A.
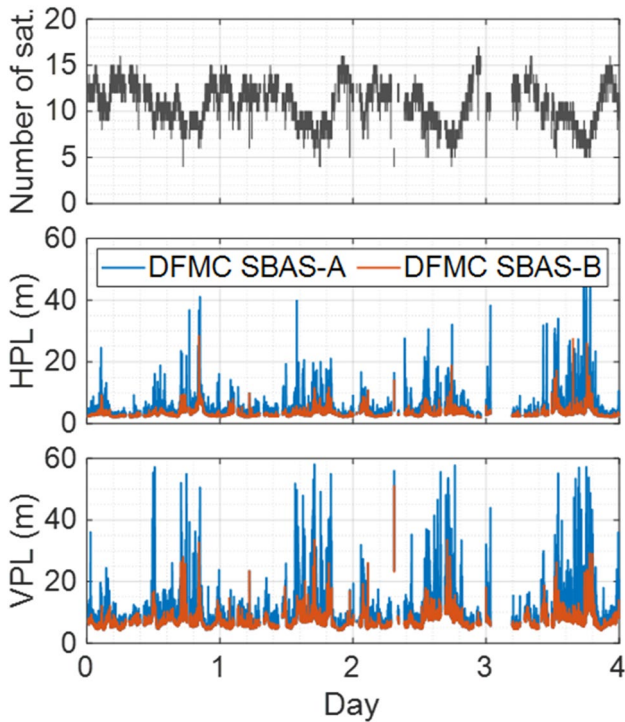
Fig. 10 Number of satellites (top) and the user protection levels in terms of HPL (middle) and VPL (bottom) on the disturbed days at the CNBR station (Day 1 to 4 represents DOY 36, 38, 45, and 50 in 2022)
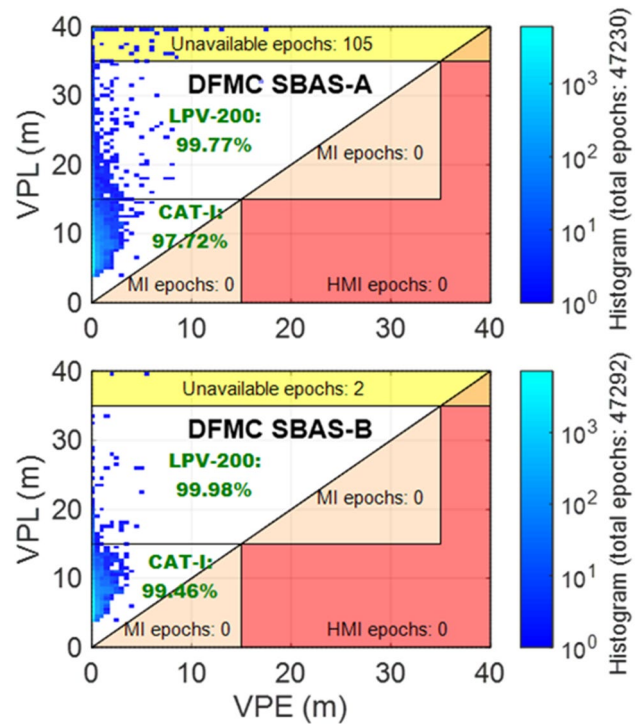
DFMC SBAS performances for LPV-200 and CAT-I phases

Finally, the ICAO requirements of the PA model (ICAO SARPS 2006) are considered. For the LPV-200 (equivalent CAT-I) and CAT-I categories, the vertical alert limit (AL) bounds are determined as 35 and 15 m, respectively. In the assessments of DFMC SBAS, both the positioning errors and protection levels are plotted in the Stanford diagram.

Figure 12 compares the Stanford diagrams between the DFMC SBAS-A and DFMC SBAS-B methods at the user station (CNBR) on four quiet days. The MI and HMI stand for misleading information and the hazard misleading information, respectively. The color bar indicates the values of the histogram for four days. The availabilities of DFMC SBAS-A in the LPV-200 and CAT-I categories are about 99.77% and 97.72%, and of DFMC SBAS-B in both categories are 99.98% and 99.46%, respectively. Evidently, the DFMC SBAS-B method can improve the DFMC SBAS-A method by 0.21% and 1.74% with the LPV-200 and CAT-I categories, respectively.

Table 2 shows the summarized availabilities of DFMC SBAS for three users. As expected, the local ionospheric disturbances decrease the availability at each user station. On the disturbed days, the available percentages are reduced depending on the baselines between the users and the master

Fig. 11 95.th percentile HPL (top panel) and VPL (bottom panel) on the quiet (left panel) and disturbed (right panel) days for three user stations (CNBR, UTTD, and SRTN)

Fig. 12 Stanford diagrams of the DFMC SBAS-A (top) and DFMC SBAS-B (bottom) methods at the CNBR station on the four quiet days

Table 2 Available percentages of the DFMC SBAS-B/DFMC SBAS-A methods at the CNBR, UTTD, and SRTN stations for the LPV-200 and CAT-I categories, respectively

Stations	Baselines (km)	LPV-200 (%)		CAT-I (%)	
		Quiet	Disturbed	Quiet	Disturbed
CNBR	60	99.98/99.77	99.71/99.42	99.46/97.72	97.75/95.53
UTTD	432	99.98/99.74	99.70/98.32	99.18/96.99	97.42/94.80
SRTN	529	99.98/99.74	99.70/98.35	99.21/96.93	97.20/94.42

station. For example, the available (%)/baselines (km) in CAT-I are about 97.75/60, 97.42/432, and 97.20/529 at the CNBR, UTTD, and SRTN stations, respectively. Note that the baselines can reduce the availability below 1%. Additionally, if we assess the available percentages in LPV-200 and CAT-I with the ICAO requirements of 99.99%, the available DFMC SBAS with the method B in Thailand cannot yet be achieved.

We can roughly divide the correction of the HOI delay problem into: receiver-end (user) processing of satellite signals and the base (master) station or control center processing of satellite signals. At the master station, the HOIs need to be removed from the residual errors, then the DFMC SBAS corrections (satellite orbit errors, satellite clock errors) are generated. In the process, the estimated HOI delays of each satellite need to be computed at each reference station. On the other hand, on the receiver side, the HOIs need to be estimated and removed from the pseudorange observations. As space weather plays an important role in the variation of ionospheric delays, HOI included, both types of processing need to consider the influencing factors of the HOIs such as solar activity, geomagnetic activity and other space weather parameters. The annual, seasonal and temporal variation of HOIs need to studied and, importantly, HOI models should be developed. Location (latitude and longitude) factors are also of importance. During the upcoming solar maximum, the ionospheric delays tend to increase and during geomagnetic storms typically as a result of solar flare events, the ionospheric irregularity (EPB events) often occurs, hence, more data collection and analysis are continually required. The master and receiver sides will benefit from such HOI models. With disturbance detection, both the receiver and the master station can adapt to more accurate HOI values.

Conclusion

In this work, we evaluate the DFMC SBAS with and without the HOI mitigation in Thailand. The procedures for local DFMC SBAS corrections and integrity parameters are proposed and then generated by using the local GNSS reference stations. The estimated local HOI delays are used in the HOI mitigation showing that the improvements of user positioning errors are up to in 13%, but the improvements on the disturbed days are slightly less than those on the quiet days. The results on the protection levels follow the trends of positioning errors. The availability of DFMC SBAS with the local DFMC SBAS corrections for both LPV-200 and CAT-I categories are 99.98% and 99.46%, respectively. It is worth noting that the suitable SBAS operation with the customer requirements must be below 99%. The HOI mitigation is hence beneficial to DFMC SBAS operation. Further studies and analyzes of DFMC SBAS during the upcoming solar maximum need to be made together with advanced algorithms and multi-constellations to achieve availability levels according to ICAO standards.

In addition, the integrity parameter (UIRE) needs to be created for the (new) regional model based on the actual observations and the local ionospheric disturbances. The regional model will improve the performance of DFMC SBAS particularly on a local scale.

Author contributions All authors contributed to the study conception and design. Material preparation, data collection and analysis were performed by SS, PS, and LMMM. The first draft of the manuscript was written by SS. The data preparation and analysis and manuscript are performed by SS. The idea generations in early versions are jointly made by SS and PS. Later refinement of proposed methods is additionally suggested and discussed in detail by SS and LMMM. Manuscript preparation and many updates are jointly accomplished by all authors.

Declarations

Competing interests   The authors declare no competing interests.

Open Access   This article is licensed under a Creative Commons Attribution 4.0 International License, which permits use, sharing, adaptation, distribution and reproduction in any medium or format, as long as you give appropriate credit to the original author(s) and the source, provide a link to the Creative Commons licence, and indicate if changes were made. The images or other third party material in this article are included in the article's Creative Commons licence, unless indicated otherwise in a credit line to the material. If material is not included in the article's Creative Commons licence and your intended use is not permitted by statutory regulation or exceeds the permitted use, you will need to obtain permission directly from the copyright holder. To view a copy of this licence, visit http://creativecommons.org/licenses/by/4.0/.

References

European GNSS Agency (2018) GNSS User Technology Report Issue 2. DOI: https://doi.org/10.2878/743965.

Guo J, Qi L, Liu X, Chang X, Ji B, Zhang F (2023) High-order ionospheric delay correction of GNSS data for precise reduced-dynamic determination of LEO satellite orbits: cases of GOCE, GRACE, and SWARM. GPS Solutions. https://doi.org/10.1007/s10291-022-01349-6

Hadas T, Krypiak-Gregorczyk A, Hernández-Pajares M, Kaplon J, Paziewski J, Wielgosz P, Orus-Perez R (2017) Impact and implementation of higher-order ionospheric effects on precise GNSS applications. J Geophys Res Solid Earth 122(11):9420–9436

Hoque MM, Jakowski N (2007) Higher order ionospheric effects in precise GNSS positioning. J Geodesy 81(4):259–268

ICAO (2018) DFMC SBAS SARPS - Baseline draft for validation. Int. Civil Aviation Org, https://www.icao.int/airnavigation/Pages/DFMC-SBAS.aspx.

Jie CHEN, Zhigang HUANG, Rui LI (2018) Computation of satellite clock-ephemeris augmentation parameters for dual-frequency multi-constellation satellite-based augmentation system. J Syst Eng Electron 29(6):1111–1123

Jürgen M, Oliver B, Katrin T, Kirsten E, Claudia S (2021) Geomagnetic Kp index. V. 1.0. GFZ Data Services, https://doi.org/10.5880/Kp.0001, https://kp.gfz-potsdam.de/en/

Krypiak-Gregorczyk A, Wielgosz P (2018) Carrier phase bias estimation of geometry-free linear combination of GNSS signals for ionospheric TEC modeling. GPS Solutions. https://doi.org/10.1007/s10291-018-0711-4

Li R, Zheng S, Wang E, Chen J, Feng S, Wang D, Dai L (2020) Advances in BeiDou navigation satellite system (BDS) and satellite navigation augmentation technologies. Satell Navig 1(12):1–23. https://doi.org/10.1186/s43020-020-00015-x

Liu Z, Li Y, Guo J, Li F (2016) Influence of higher-order ionospheric delay correction on GPS precise orbit determination and precise positioning. Geodesy Geodyn 7(5):369–376

Malys S, Slater J (1994) Maintenance and enhancement of the World Geodetic System 1984. In: Proceedings of the 7th International Technical Meeting of the Satellite Division of The Institute of Navigation (ION GPS 1994):17–24.

Marques HA, Monico JF, Aquino M (2011) RINEX_HO: second-and third-order ionospheric corrections for RINEX observation files. GPS Solutions 15(3):305–314

Nose M, Iyemori T, Sugiura M, Kamei T (2015) World data center for geomagnetism. Kyoto, Geomagnetic Dst Index. https://doi.org/10.17593/14515-74000

Ogier E (2021) Stanford Diagram. MATLAB Central File Exchange. https://www.mathworks.com/matlabcentral/fileexchange/86383-stanford-diagram

Qi L, Guo J, Xia Y, Yang Z (2021) Effect of higher-order ionospheric delay on precise orbit determination of GRACE-FO based on satellite-borne GPS technique. IEEE Access 9:29841–29849

Reid T, Walter T, Enge P (2013a) Qualifying an L5 SBAS MOPS ephemeris message to support multiple orbit classes. In: Proceedings of the 26th International Technical Meeting of the Satellite Division of the Institute of Navigation (ION GNSS+ 2013) :825–843

Reid T, Walter T, Enge P (2013b) L1/L5 SBAS MOPS ephemeris message to support multiple orbit classes. In: Proceedings of the 2013 International Technical Meeting of The Institute of Navigation 0(0):78–92.

RTCA DO-229D (2006) Minimum Operational Performance Standards for Global Positioning System/Wide Area Augmentation System Airborne Equipment. document RTCA DO-229D, RTCA Inc., Washington, DC 20036 USA

ICAO SARPS (2006) Annex 10: International Standards and Recommended Practices. Aeronautical Telecommunications, Int. Civil Aviation Org., Montréal, QC, Canada

Schaer S (1999) Mapping and Predicting the Earth's Ionosphere Using the Global Positioning System. Ph.D. dissertation Astronomical Institute University of Berne

Setti P D T, Alves D B M, Silva C M D (2019) Klobuchar and Nequick G ionospheric models comparison for multi-GNSS single-frequency code point positioning in the Brazilian region. Boletim de Ciências Geodésicas 25(0)

Shao B, Ding Q, Wu X (2020) Estimation method of SBAS dual-frequency range error integrity parameter. Satell Navig 1(1):1–8

Sickle JV, Dutton JA (2020) GEOG 862: GPS and GNSS for Geospatial Professionals. Penn State's College of Earth and Mineral Sciences, https://www.e-education.psu.edu/geog862/print/book/export/html/1727

Sophan S, Myint L M, Supnithi P (2022) Preliminary Evaluations of User Positioning Errors in DFMC SBAS Demo at Thailand Location. In: Proceedings of the IWAC2022 0(0):49–54

Subirana J, Zornoza J, Hernández-Pajares M (2013) GNSS Data Processing-Volume I: Fundamentals and algorithms. European Space Agency, https://gssc.esa.int/navipedia/GNSS_Book/ESA_GNSS-Book_TM-23_Vol_I.pdf

Takahashi T, Saito S, Kitamura M, Sakai T (2022) Performance of DFMC SBAS broadcasted from Japanese QZSS in Oslo, Norway. In: Proceedings of the 2022 International Technical Meeting of The Institute of Navigation:401–406

Takasu T (2013) RTKLIB ver. 2.4. 2 Manual. RTKLIB: An Open Source Program Package for GNSS Positioning

Xi K, Wang X (2021) Higher order ionospheric error correction in BDS precise orbit determination. Adv Space Res 67(12):4054–4065

Yehun A, Kassa T, Vermeer M, Hunegnaw A (2020) Higher order ionospheric delay and derivation of regional total electron content over ethiopian global positioning system stations. Adv Space Res 66(3):612–630

Zhao L, Hu X, Tang C, Cao Y, Zhou S, Yang Y, Guo R (2020) Generation of DFMC SBAS corrections for BDS-3 satellites and improved positioning performances. Adv Space Res 66(3):702–714

Somkit Sophan is currently a postdoctoral researcher at King Mongkut's Institute of Technology Ladkrabang (KMITL), Thailand. He received his B.S. and M.S. degrees in electronic and electrical engineering from the Rajamangala University of Technology Isan, Thailand, in 2015 and 2017, and his Doctor of Engineering from KMITL in 2023. His research interests include the GNSS positioning and developments of the SBAS technology.

Pornchai Supnithi is a full professor at King Mongkut's Institute of Technology Ladkrabang, Thailand. He is interested in Ionospheric study and GNSS and Data storage technology. His laboratory maintains ionospheric monitoring stations in Thailand (ionosonde, VHF radar, beacon receivers, GNSS receivers) and Thai GNSS and Space Weather Information Website. He has published over 60 international journals and 3 books/chapters.

Lin M. M. Myint is currently an assistant professor at King Mongkut's Institute of Technology Ladkrabang, Thailand, and a member of Thai GNSS and Space Weather Information Data Center. His research interests are in signal processing on data storage and communications, space weather analysis, and GNSS positioning and navigation.

Susumu Saito is currently a Principal Researcher with the Electronic Navigation Research Institute, National Institute of Maritime, Port, and Aviation Technology, Tokyo, Japan. His research interests include ionospheric effects on GNSS, the development of GNSS ground-based augmentation system suitable for the low-latitude region, and ionospheric sciences using radio and optical techniques.

Kornyanat Hozumi is a researcher at the Space Environment Laboratory, Radio Propagation Research Center, Radio Research Institute, National Institute of Information and Communications Technology (NICT), Tokyo, Japan. Her research interests include employing radio wave techniques to study the ionosphere and upper atmosphere and linking space weather research to real operation.

Michi Nishioka is a senior researcher at the Space Environment Laboratory, Radio Propagation Research Center, Radio Research Institute, National Institute of Information and Communications Technology (NICT), Tokyo, Japan. Her group monitors ionospheric conditions through ionosonde and GNSS observations. Her research interests include the ionospheric disturbances related to space weather research.